Carrier-Based PWM-VSI Overmodulation Strategies: Analysis, Comparison, and Design

Ahmet M. Hava, *Student Member, IEEE,* Russel J. Kerkman, *Fellow, IEEE,* and Thomas A. Lipo, *Fellow, IEEE*

***Abstract*— In this paper, the overmodulation region voltage-gain characteristics and waveform quality of carrier-based pulsewidth-modulated (PWM) methods are investigated. Through detailed analytical study, voltage-gain characteristics are extracted independent of carrier frequency. The influence of blanking time and minimum pulsewidth (MPW) control on the inverter gain characteristics are studied and shown to be significant. A comparative evaluation of the modulator characteristics reveals the advantageous high-modulation-range characteristics of discontinuous PWM methods and, in particular, the superior overmodulation performance of a discontinuous PWM method. The modulation methods under consideration are tested on a PWM voltage-source inverter (VSI)-fed induction motor drive in the laboratory, and the theoretical results are verified by experiments. Also, a gain linearization technique is presented and experimentally verified. The results of this study are useful in design, performance prediction, and development of high-performance overmodulation strategies for PWM-VSI drives.**

***Index Terms*— Current harmonics, inverter, overmodulation, voltage gain.**

I. Introduction

PULSEWIDTH-modulated (PWM) voltage-source inverters (VSI's) are widely utilized in ac motor drive applications and at a smaller quantity in controlled rectifier applications as a means of dc $\Leftrightarrow$ ac power conversion devices. Many PWM-VSI drives employ carrier-based PWM methods due to their fixed switching frequency, low ripple current, and well-defined harmonic spectrum characteristics. Utilizing the conventional VSI structure shown in Fig. 1, which has eight discrete voltage-output states, carrier-based PWM methods program a "per carrier cycle average output voltage" equal to the reference voltage. Employing the triangle-intersection technique [1] or direct digital pulse programming technique [2], carrier-based PWM methods provide a linear relationship between the reference and output voltages within a limited range.

The linear voltage range of a PWM-VSI drive is mainly determined by the modulator characteristics. Inverter blanking time and minimum-pulsewidth constraints can further reduce the range of linearity by a considerable amount. As a result, the voltage linearity of a drive, for example, in the sinusoidal PWM (SPWM) case, can be lost at as low a value as 70% of the six-step voltage. Fig. 2 illustrates the typical linear and nonlinear range modulation waveforms of the SPWM method and switching device gate logic signals. The portion of the modulation wave having a larger magnitude than the triangular wave peak value remains unmodulated, and the gate signals remain on or off for a full carrier cycle leading to a nonlinear reference output-voltage relationship.

Operating in the nonlinear modulation range, or in more common terms, the overmodulation range is problematic: 1) large amounts of subcarrier frequency harmonic currents are generated; 2) the fundamental component voltage gain significantly decreases; and 3) the switching device gate pulses are abruptly dropped. In constant V/f-controlled PWM-VSI induction motor drives, operation in this range results in poor performance, and frequent overcurrent fault conditions occur. In current-controlled drives, in addition to the inherent modulator subcarrier frequency harmonic-distortion-dependent waveform degradation, current-regulator-dependent performance reduction results. The current regulators are heavily burdened by the feedback current subcarrier frequency harmonics and regulator saturation and oscillatory operations result in additional performance degradation. On the other hand, full inverter voltage utilization is important from cost and power density improvement perspectives. Also, a drive with high-performance overmodulation range operating capability is less sensitive to inverter dc-bus voltage sag, which often occurs in diode-rectifier front-end-type drives due to ac-line voltage sag or fault conditions, hence, increased drive reliability. Recently, overmodulation issues have attracted the attention of many researchers, and overmodulation strategies for the two popular methods—SPWM [3], [4] and space-vector PWM (SVPWM) [5], [6]—have been developed. However, the overmodulation characteristics of many other carrier-based PWM methods have not been explored, nor has a comparative study been reported.

This study investigates the overmodulation range voltage-gain characteristics and waveform quality of several popular carrier-based PWM methods employing the triangle-intersection technique. The detailed comparative study reveals the advantageous attributes of a discontinuous modulation wave PWM method, and a simple gain linearization technique provides modulator linearity until the six-step mode. The theoretical results are verified by laboratory experiments.

Manuscript received September 17, 1996; revised June 8, 1997. Recommended by Associate Editor, D. Torrey.

A. M. Hava is with Yaskawa Electric America, Inc., Northbrook, IL 60062-2028 USA.

R. J. Kerkman is with Rockwell Automation-Allen Bradley, Mequon, WI 53092-0760 USA (e-mail: rjkerkman@meq1.ra.rockwell.com).

T. A. Lipo is with the Electrical and Computer Engineering Department, University of Wisconsin, Madison, WI 53706-1691 USA (e-mail: hava@cae.wisc.edu; lipo@engr.wisc.edu).

Publisher Item Identifier S 0885-8993(98)04851-0.

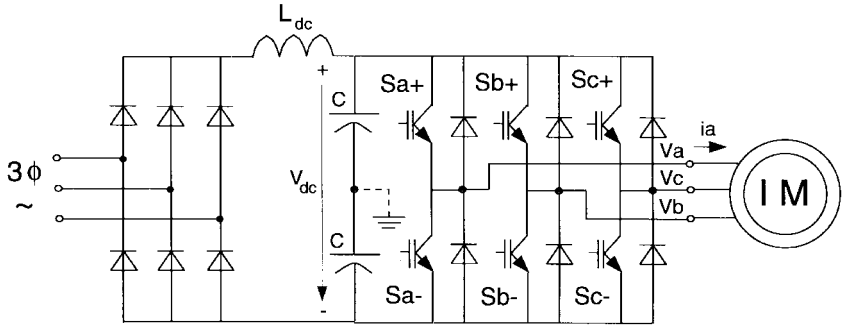

Fig. 1. Main power converter structure of the widely utilized diode-rectifier front-end-type PWM-VSI drive.

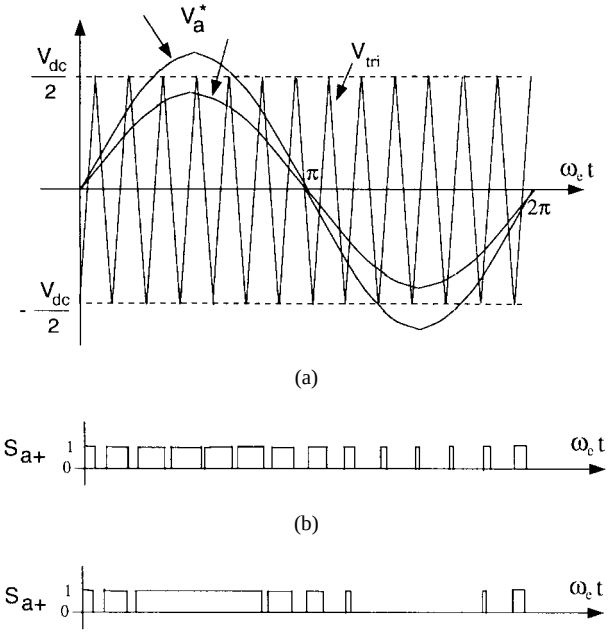

Fig. 2. SPWM modulation waveforms and switching device gate logic signals. (a) Linear modulation range. (b) Overmodulation range.

II. Review of Carrier-Based PWM Methods

There are two widely utilized carrier-based PWM implementation techniques: the direct digital gate pulse programming technique and the triangle-intersection technique. In the direct method, the gate signal on-state times t_a^*, t_b^*, and t_c^* are calculated from the space-vector voltage equation and directly programmed. The space-vector PWM methods, which vary depending on the partitioning of two inverter zero states, generally employ the direct method [2], [7].

In the triangle-intersection technique [1], three reference modulation waves v_a^*, v_b^*, and v_c^* are compared with triangular carrier waves to generate the switch gate signals. In isolated neutral-type loads, the freedom to add a zero-sequence signal to the modulation waves leads to a large variety of modulation waves, hence modulation methods [8], [9]. As shown in Fig. 3, in the zero-sequence signal injection method, the reference modulation waves v_a^*, v_b^*, and v_c^* are utilized to compute a zero-sequence signal V_0. Adding V_0 to the original reference signals, the modified reference signals v_a^{**}, v_b^{**}, and v_c^{**} are obtained, and comparing these signals with the carrier wave yields the gate signals. In addition to SPWM [1], several high-performance zero-sequence signal injection methods such as the third-harmonic injection PWM (THIPWM) [10], Depenbrock's discontinuous PWM (DPWM1) method [11], [12], and the zero-sequence signal injection method equivalent of the conventional SVPWM method [13], [14] also employ the triangle-intersection technique. The triangle-intersection technique has been traditionally implemented by analog hardware. Recently, various microprocessors (μP) and digital signal processor (DSP) chips with built-in fully digital triangle-intersection-based PWM capability have been developed and found a wide range of applications in fully digital PWM-VSI drives. In this study, triangle-intersection-based techniques will be considered. Although the overmodulation switching patterns of the direct digital implemented PWM methods may be quite similar to triangle-intersection implementations of PWM methods, the overmodulation strategies of the direct digital method [5], [6] are quite different and more complex.

With simplicity and the degree of improvement over the existing methods as the main criteria, of the many methods developed, only a small number of modulation methods have gained wide acceptance [9]. Due to its simplicity, the SPWM method has found a wide range of applications. The conventional SVPWM, its triangle-intersection implementation, and THIPWM methods are preferred in high-performance drives due to the wider linear range and reduced carrier frequency harmonic distortion characteristics they provide compared to the SPWM method. Two modulators with discontinuous modulation waves, classified as discontinuous PWM (DPWM), Depenbrock's DPWM1 [11], and Ogasawara's DPWM2 [7] methods, have gained recognition due to their low harmonic distortion at high-voltage utilization and the controllability of the switching losses [8]. The first implementation of DPWM2 employed the direct digital implementation technique, while the triangle-intersection implementation and therefore the modulation wave appeared in the following years [15]. Fig. 4 shows the modulation waves of the discussed modulators at 72% of the six-step voltage. In the figure, unity triangular carrier wave gain is assumed, and the modulation signals are normalized to $\frac{V_{dc}}{2}$. Therefore, $\pm\frac{V_{dc}}{2}$ saturation limits correspond to ± 1. The overmodulation voltage-gain characteristics of these modulators will be investigated in detail in this paper.

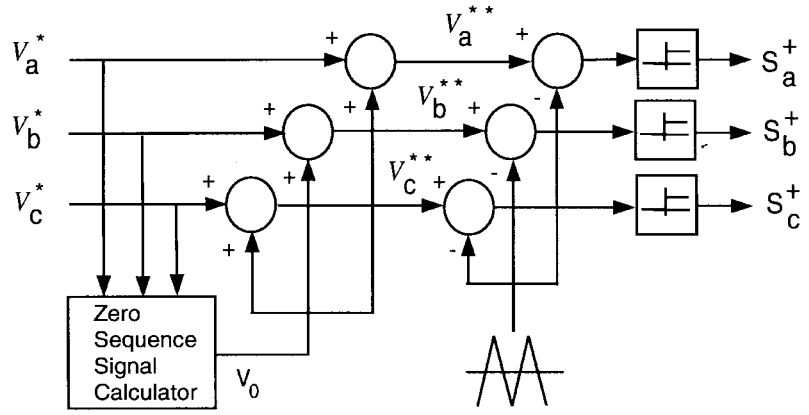

Fig. 3. Triangle-intersection technique-based generalized zero-sequence injection PWM diagram.

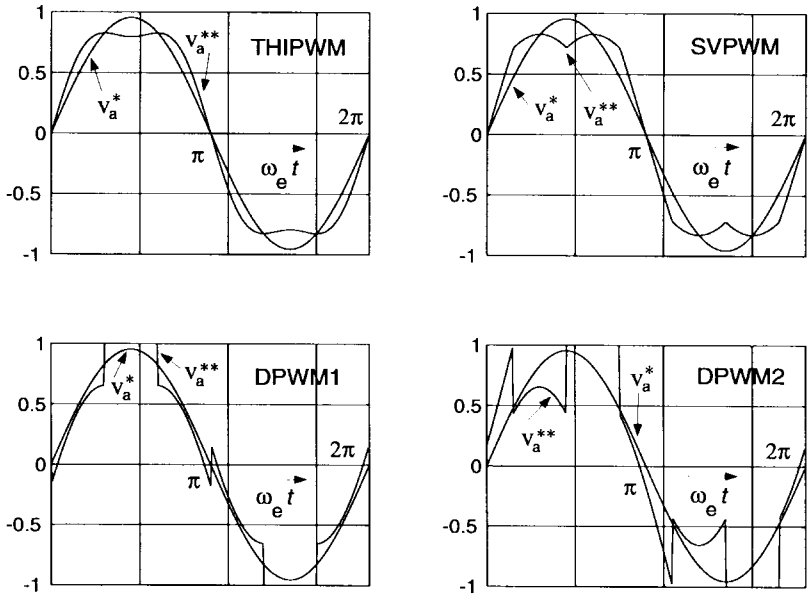

Fig. 4. Modulation waveforms of the popular PWM methods ($M_i = 0.72$).

The voltage linearity, harmonic distortion, and overmodulation range performance characteristics of a modulator are mainly dependent on the voltage-utilization level, i.e., modulation index. At this stage, a modulation index definition is required. For a given dc-bus voltage $V_{\rm dc}$, the ratio of the fundamental component magnitude of the line to neutral inverter output voltage V_{1m} to the fundamental component magnitude of the six-step mode voltage $\frac{2V_{\rm dc}}{\pi}$ is termed the modulation index M_i [9]

$$M_i = \frac{V_{1m}}{\frac{2V_{\rm dc}}{\pi}}. \tag{1}$$

Using this definition, full voltage utilization (six-step operating mode) occurs at $M_i = 1$. Normalizing the triangular wave peak-to-peak signal magnitude to $V_{\rm dc}$, it follows that SPWM's linear modulation range ends at $V_{1m} = \frac{V_{\rm dc}}{2}$, a modulation index of $M_{i\,\max[\rm SPWM]} = \frac{\pi}{4} \approx 0.785$. The voltage linearity of a modulator can be significantly increased by injecting a zero-sequence signal. The theoretical limit of SVPWM can be easily calculated by evaluating the modulation signal at the 60° point, where the zero-sequence signal becomes zero and this calculation yields $M_{i\,\max[\rm PWM]} = \frac{\pi}{2\sqrt{3}} \approx 0.907$. The theoretical linearity limit of all the discussed zero-sequence injection PWM methods is equal to this inverter theoretical limit.

Within the lower portion of the linear modulation range, SPWM, SVPWM, and THIPWM demonstrate better performance characteristics than the two discontinuous PWM methods, while in the high-modulation region, the opposite is true [8]. In addition, with the discontinuous PWM methods, the modulator characteristics have significant influence on the inverter switching losses: under the same inverter average switching frequency criteria, DPWM1 has reduced losses for unity power factor loads [15], and DPWM2 has reduced losses for 30° lagging loads [7], [15] compared to SPWM and SVPWM. Therefore, the linear modulation range performance of a PWM-VSI drive can be enhanced by selecting SPWM, THIPWM, or SVPWM in the low-modulation range, and DPWM1 or DPWM2 in the high-linear-modulation range. However, at this point it is not clear which modulator has better performance in the overmodulation range. Also, the influence of inverter nonidealities such as blanking time and minimum pulsewidth (MPW) control on the linearity limit

of a modulator is not quantified. From the perspective of optimizing the overall performance, the overmodulation range performance characteristics of these modulation methods must be evaluated. This paper is dedicated to a detailed study of the overmodulation region.

III. Overmodulation Range Voltage-Gain Characteristics

In the triangle-intersection technique, when the modulation wave magnitude becomes larger than the peak of the triangular wave, switching during that carrier cycle ceases and the corresponding switch remains locked to the inverter pole within the carrier cycle. In the beginning of the overmodulation region, depending on the modulator type, one or two of the three modulation waves are simultaneously saturated. As the modulation index increases, the saturated segments of each modulation wave and the number of simultaneously saturated phases increase according to the waveform characteristic of each modulator until the six-step mode is reached.

When saturation occurs, the reference per carrier cycle average voltage cannot be matched by the inverter, and a voltage-gain reduction results. This nonlinear voltage-gain relation can be analytically modeled by Fourier analysis of the saturated modulation wave independently of the carrier frequency. The voltage gain calculated with this method is highly accurate. Detailed computer simulations indicated for $\frac{f_c}{f_e} > 20$, the relative gain error is less than 0.5% and the error significantly decreases with increasing $\frac{f_c}{f_e}$. Since the widely utilized PWM-VSI drives employing insulated gate bipolar transistor (IGBT) devices typically have high $\frac{f_c}{f_e}$ values, the model successfully represents most inverter drives. Utilizing the modulation index definition, general formulas can be derived independent of the inverter voltage. Except for the SPWM method, the voltage-gain formulas of the carrier-based PWM methods have not been reported, nor has a detailed gain characteristic study been conducted [4], [16]. In the following, the gain formulas of the discussed modulators are derived, and a comparative evaluation follows.

The fundamental component voltage gain of a modulator is the ratio of the output-voltage fundamental component peak value V_{1m} to the reference modulation wave fundamental component peak value V_m^*. Utilizing the modulation index and reference modulation index definitions, it can also be expressed in terms of the modulation indexes as

$$G = \frac{V_{1m}}{V_m^*} = \frac{M_i}{M_i^*}. \tag{2}$$

The gain formulas developed below have the following applications:

1) fundamental component VSI overmodulation modeling;
2) linearizing the inverter gain block in the controller;
3) they provide simple tools for gain analysis and comparisons of modulators.

A. Sinusoidal PWM

The fundamental component of the saturated sinusoidal modulation wave can be calculated by employing Fourier analysis, and the result can be expressed in terms of the modulation index relations in the following [4], [16]:

$$M_i = \left(\frac{2}{\pi}\right) M_i^* \arcsin\left(\frac{\pi}{4M_i^*}\right) + \left(\frac{1}{2}\right)\sqrt{1-\left(\frac{\pi}{4M_i^*}\right)^2}. \tag{3}$$

Since the output-voltage fundamental component is different from the reference voltage, the output modulation index M_i has a different value from the reference modulation index M_i^*. Utilizing the definition of (2), the fundamental component voltage relation can be expressed by the following gain function:

$$G = \left(\frac{2}{\pi}\right) \arcsin\left(\frac{\pi}{4M_i^*}\right) + \left(\frac{1}{2M_i^*}\right)\sqrt{1-\left(\frac{\pi}{4M_i^*}\right)^2}. \tag{4}$$

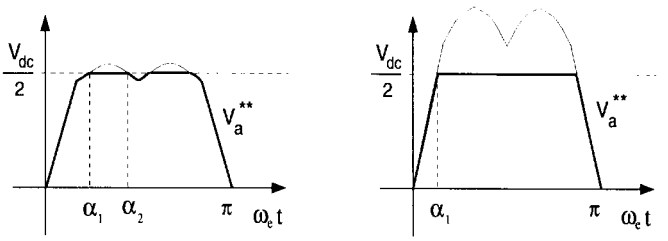

(a) (b)

Fig. 5. SVPWM triangle-intersection method modulation waveforms in the overmodulation region. (a) Region I. (b) Region II.

B. Space-Vector PWM

Generating the modulation wave of conventional SVPWM method is quite simple. Of the three sinusoidal modulation waves, the one with the smallest magnitude is multiplied by a coefficient of $\frac{1}{2}$ to generate the zero-sequence signal [14]. Adding this signal to all the reference waves results in a modulation wave which is very similar to THIPWM modulation wave. The overmodulation range characteristics of the triangle-intersection implementation of the SVPWM, therefore, can be closed-form modeled in the same manner as SPWM. As illustrated in Fig. 5, the overmodulation region consists of two subregions. Region I has two intersections between the saturation line and the modulation waveform per quarter wave while Region II has only one intersection. Employing Fourier analysis, the fundamental component modulation index and voltage-gain relations of overmodulation Region I are found as follows:

$$M_i = -\frac{1}{2}M_i^* + \frac{3}{\pi}M_i^* \arcsin\left(\frac{\pi}{2\sqrt{3}M_i^*}\right) + \frac{\sqrt{3}}{2}\sqrt{1-\left(\frac{\pi}{2\sqrt{3}M_i^*}\right)^2} \tag{5}$$

$$G = -\frac{1}{2} + \frac{3}{\pi}\arcsin\left(\frac{\pi}{2\sqrt{3}M_i^*}\right) + \frac{\sqrt{3}}{2M_i^*}\sqrt{1-\left(\frac{\pi}{2\sqrt{3}M_i^*}\right)^2}. \tag{6}$$

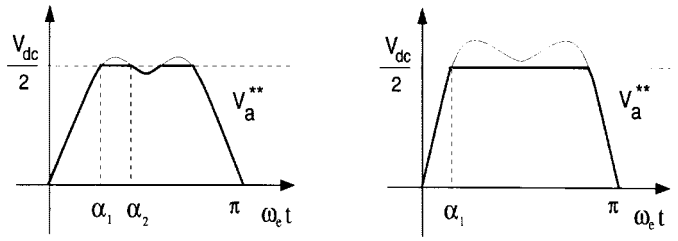

Fig. 6. THIPWM waveforms in the overmodulation region. (a) Region I. (b) Region II.

Region II begins at $M_i^* = \frac{\pi}{3} \approx 1.047$ ($M_i \approx 0.957$), and the modulation index and gain relations in this region are calculated as follows:

$$M_i = \frac{3}{\pi} M_i^* \arcsin\left(\frac{\pi}{6M_i^*}\right) + \frac{1}{2}\sqrt{1-\left(\frac{\pi}{6M_i^*}\right)^2} \quad (7)$$

$$G = \frac{3}{\pi}\arcsin\left(\frac{\pi}{6M_i^*}\right) + \frac{1}{2M_i^*}\sqrt{1-\left(\frac{\pi}{6M_i^*}\right)^2}. \quad (8)$$

C. Third-Harmonic Injection PWM

The zero-sequence signal of THIPWM can be algebraically defined as $v_0 = \frac{1}{6}V_{1m}\sin(3w_e t)$ [10]. The overmodulation voltage-gain relations of this method are quite similar to the SVPWM methods.

As shown in Fig. 6(a), in Region I, the modulator waveform intersects with the saturation line twice per quarter-fundamental cycle. The intersection angles are calculated from the following transcendental equation:

$$\sin\alpha_{1,2} + \frac{1}{6}\sin 3\alpha_{1,2} = \frac{\pi}{4M_i^*}. \quad (9)$$

The above equation can be easily solved by iterative methods. Utilizing the intersection angle values, the reference output-voltage relationship can be computed by the following formula established by the Fourier analysis of the modulation wave:

$$M_i = \left(\frac{2}{\pi}\right) M_i^* \left(\frac{\pi}{2} + \alpha_1 - \alpha_2 + \frac{5}{12}(\sin 2\alpha_2 - \sin 2\alpha_1) + \frac{1}{24}(\sin 4\alpha_2 - \sin 4\alpha_1)\right) + \cos\alpha_1 - \cos\alpha_2. \quad (10)$$

The above formula is valid until the reference modulation index value of $M_i^* = \frac{3\pi}{10} \approx 0.943$ and then Region II begins while in Region II, only one intersection point exists and can be calculated from (9). Finally, the modulation index can be calculated from the Fourier analysis derived formula as follows:

$$M_i = \left(\frac{2}{\pi}\right) M_i^* \left(\alpha_1 - \frac{5}{12}\sin 2\alpha_1 - \frac{1}{24}\sin 4\alpha_1\right) + \cos\alpha_1. \quad (11)$$

Although the above formulas are dependent on the intersection angles and difficult to completely write in full closed form, they can be easily evaluated by simple numerical software packages. Once the modulation index values are calculated, the gain can be easily computed from (2).

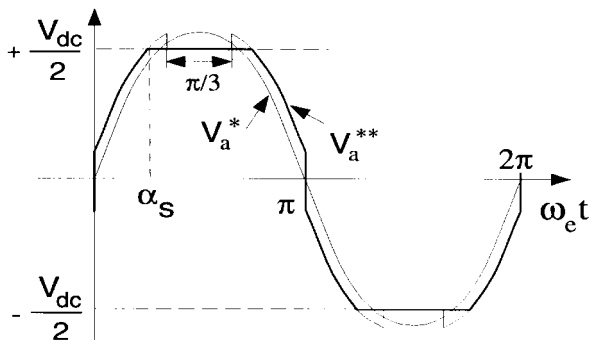

Fig. 7. DPWM1 method overmodulation waveforms.

The third-harmonic injection PWM method with a slightly better linear modulation region waveform quality than the above method ($v_0 = \frac{1}{4}V_{1m}\sin(3w_e t)$ [17]) loses linearity at $M_i^* = \frac{3\sqrt{3}}{7\sqrt{7}}\pi \approx 0.885$, and its overmodulation gain characteristic can be evaluated following the same algebraic steps described in this section. The gain characteristic of this modulator is very similar to the conventional THIPWM method, and further details can be found in [18].

D. Depenbrock's Discontinuous PWM Method (DPWM1)

In this fairly old method [11], [12], the zero-sequence signal generation steps are simple. Of the three reference sinusoidal modulation waves, the one with the largest magnitude determines the zero sequence. The difference between the dc-bus rail with the same polarity as this modulation wave and the modulation wave is equal to the zero-sequence signal. Assume that v_a^* is the signal with the largest magnitude. Then, $v_0 = (\mathrm{sign}(v_a^*))\frac{V_{dc}}{2} - v_a^*$. Adding such a zero sequence to the reference signals, discontinuous modulation waves with two 60° saturated segments result. As shown in Fig. 7, once in the overmodulation range, the saturated segments increase beyond the 60° value of the linear modulation range, and the modulation wave is upward shifted by an amount dependent on the modulation index value. Fourier analysis of the saturated wave yields the following:

$$M_i = -1 + \left(\frac{\sqrt{3}}{\pi} - \frac{1}{2}\right) M_i^* + \left(\frac{\pi}{4\sqrt{3}}\right)\frac{1}{M_i^*} + \left(\frac{3}{\pi}\right) M_i^* \arcsin\left(\frac{\pi}{2\sqrt{3}M_i^*}\right) + \left(\frac{\sqrt{3}}{2}\right)\sqrt{1-\left(\frac{\pi}{2\sqrt{3}M_i^*}\right)^2} \quad (12)$$

$$G = \frac{-1}{M_i^*} + \left(\frac{\sqrt{3}}{\pi} - \frac{1}{2}\right) + \left(\frac{\pi}{4\sqrt{3}}\right)\frac{1}{M_i^{*2}} + \left(\frac{3}{\pi}\right)\arcsin\left(\frac{\pi}{2\sqrt{3}M_i^*}\right) + \left(\frac{\sqrt{3}}{2M_i^*}\right)\sqrt{1-\left(\frac{\pi}{2\sqrt{3}M_i^*}\right)^2}. \quad (13)$$

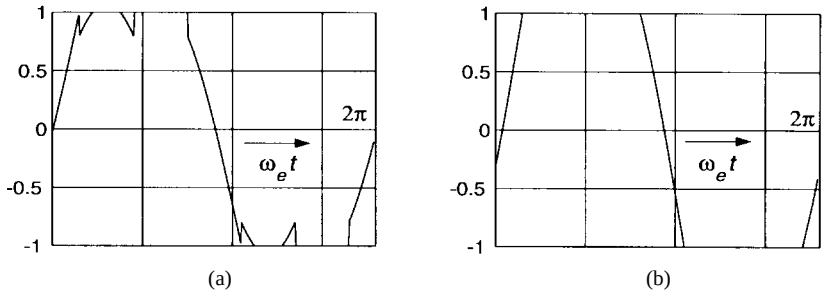

Fig. 8. DPWM2 method overmodulation waveforms. (a) Region I. (b) Region II.

E. Ogasawara's Discontinuous PWM Method (DPWM2)

In this method, the zero-sequence signal is generated in a manner similar to DPWM1. The three reference sinusoidal modulation waves are phase shifted by 30° (lagging), then the signal with the maximum magnitude defines the inverter leg to be unmodulated. The zero-sequence signal is the difference between the original modulation wave defined by the maximum magnitude test and the saturation line with the same polarity as this modulation wave. The resulting modulation wave is not quarter-wave symmetric, hence, the overmodulation voltage-gain equations are complex compared to the previous cases.

As shown in Fig. 8, the overmodulation region is divided into two subregions. In the first subregion, as shown in Fig. 8(a), the modulation wave has four saturated segments per fundamental cycle. Employing Fourier analysis and utilizing the intermediate variables ψ, a_1, and b_1, the voltage relations in the first region can be calculated from the following:

$$\psi = -\frac{\pi}{3} + \arcsin\left(\frac{\pi}{2\sqrt{3}M_i^*}\right) \tag{14}$$

$$a_1 = \frac{M_i^*}{4} - \frac{\sqrt{3}}{2}\sin\left(\psi - \frac{\pi}{6}\right) + \frac{3\psi}{2\pi}M_i^* - \frac{3}{4\pi}M_i^*\cos\left(2\psi + \frac{\pi}{6}\right) \tag{15}$$

$$b_1 = -\frac{1}{2}\cos\left(\psi + \frac{\pi}{3}\right) + \frac{\sqrt{3}}{4\pi}M_i^* \times \left(\frac{\pi}{3} - 2\psi - \sin\left(2\psi - \frac{\pi}{3}\right)\right) \tag{16}$$

$$M_i = \sqrt{a_1^2 + b_1^2}. \tag{17}$$

The second subregion begins at $M_i^* = \frac{\pi}{3}$. Shown in Fig. 8(b), the modulation wave heavily saturates, and on each side two saturated segments merge, leading to only two saturated segments per cycle. Introducing the variable α, the coefficients a_1 and b_1 can be calculated as follows:

$$\alpha = \frac{2\pi}{3} - \arcsin\left(\frac{\pi}{2\sqrt{3}M_i^*}\right) \tag{18}$$

$$a_1 = \frac{\sin\alpha}{2} + \left(\frac{1}{2} - \frac{\sqrt{3}}{8\pi} - \frac{3}{4\pi}\alpha\right)M_i^* - \frac{\sqrt{3}}{4\pi}M_i^*\cos\left(2\alpha - \frac{2\pi}{3}\right) \tag{19}$$

$$b_1 = -\frac{\cos\alpha}{2} + \frac{\sqrt{3}}{2\pi}M_i^* \times \left(\frac{\sqrt{3}}{4} - \frac{1}{2}\sin\left(2\alpha - \frac{2\pi}{3}\right) + \frac{\pi}{3} - \frac{\alpha}{2}\right). \tag{20}$$

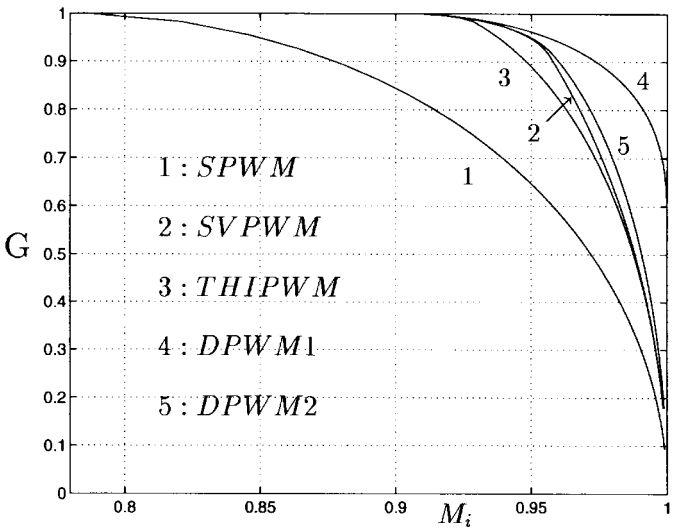

Fig. 9. The overmodulation region voltage-gain characteristics of the popular modulators.

Once the above coefficients are known, the reference output-voltage relations can be calculated from (17) and the voltage gain can be calculated in both subregions from the definition of (2).

IV. Voltage-Gain Comparisons

In this section, the voltage-gain characteristics of all the discussed modulators are comparatively evaluated. The comparisons are provided in terms of the voltage gain $[G = f(M_i)]$ and modulation index $[M_i = f(M_i^*)]$ relations. Utilizing the gain functions derived in the previous section, the gain characteristics of the candidate modulators are calculated and illustrated in Fig. 9. The improvement in the linearity range of all the zero-sequence injection methods compared to SPWM is obvious from the figure. More importantly, the graph reveals the unusual gain characteristic of Depenbrock's DPWM1 method: the gain of this modulator drops at a significantly smaller rate than all the other modulators, and the minimum value, which occurs at the six-step operating point, is $\frac{\sqrt{3}}{\pi} \approx 0.551$. All the other modulators have a rapid drop in gain, and eventually the gain becomes practically zero at the six-step operating point. The similarity of their gain characteristics with respect to each other is also obvious from the figure.

Shown in Fig. 10 and illustrated in terms of the modulation indexes, the input–output-voltage relations provide more specific information. Except for DPWM1, all the modulators

require large reference signals in order to penetrate the overmodulation region. In particular, DPWM1 requires a reference signal with a magnitude of $M_i^* = \frac{\pi}{\sqrt{3}} \approx 1.81$, while the other modulators require signals with very large magnitudes $(M_i^* \approx 5 \ldots 20)$. This result is extremely important from an implementation perspective: the smaller the gain range, the better the accuracy of the modulation signal and the smaller word length requirement of a signal processor (or the signal range in an analog implementation). Therefore, DPWM1 utilizes the signal range of a processor with high resolution and abrupt pulse dropping, and the consequent overcurrent fault condition is avoided.

The unusual gain characteristic of DPWM1 is not difficult to explain. In the overmodulation range, the zero-sequence signal of this modulator is effectively a square-wave function with an increasing magnitude as the six-step operating point is approached. Therefore, in this method, the modulation wave is vertically and horizontally forced to approach the six-step mode, while the other zero-sequence injection methods force the modulation wave to expand mainly horizontally until the six-step mode is generated. This characteristic of DPWM1 can be clearly observed in Fig. 11, where DPWM1 and SVPWM modulation waveforms are compared for a set of reference modulation index values. It is apparent that as the reference modulation index increases, the SVPWM modulation wave saturates heavily, while the DPWM1 modulation wave easily approaches the square wave.

V. Influence of Blanking Time and Minimum Pulsewidth on Modulator Gain

Inverter blanking time is the time interval that both switches of an inverter leg are open following a change in the gate logic reference signal value. It is provided for protection against the dc-bus short circuit. As shown in Fig. 12(b), the blanking time circuit delays the reference gate signals by the blanking time t_d and results in loss of gate signal symmetry (increases the uncharacteristic harmonics) and also a reduction in the output-voltage value. Typically, a gate-pulse-correction (compensation) algorithm is employed in order to restore the symmetry and volt-second balance [19]. As shown in Fig. 12(c), in the exact compensation method, if the polarity of the phase current of the corresponding inverter leg is positive (negative), the reference gate signal on the triangle side with negative (positive) slope is advanced (delayed) by the blanking time, leading to the correct output-voltage pulse.

When a modulator operates near its theoretical linearity limits, as shown in Fig. 12(a), narrow gate pulses are generated. When the width of such pulses becomes smaller than $2t_d$, the compensation algorithm fails to correct the pulses properly. In Fig. 12(c), this condition corresponds to $x \leq 0$ and correct compensation requires interference with the modulation signal in the previous half-carrier cycle. Since in the conventional digital PWM methods the reference modulation signal is generated only at the positive and/or negative peak points of the triangular carrier wave (regular sampling), correct compensation of such a narrow pulse is not possible. Hence, voltage-gain reduction occurs before the theoretical linearity

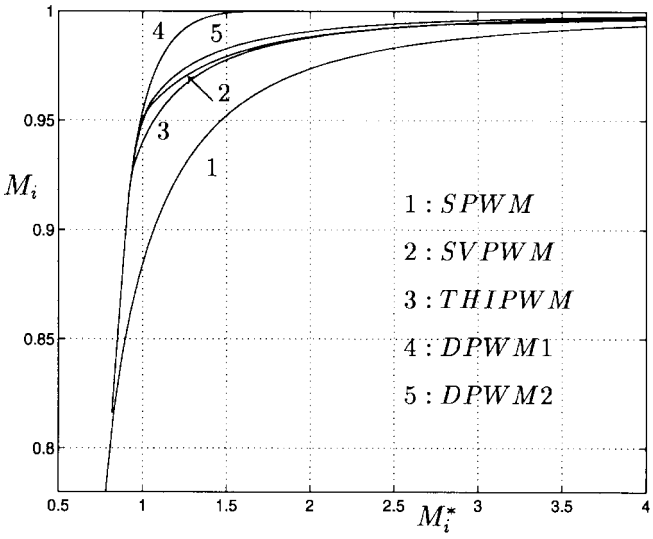

Fig. 10. Overmodulation region $M_i = f(M_i^*)$ characteristics.

limit. The lowest modulation level at which this problem occurs can be easily calculated. When the modulation signal v^* is positive, the narrow pulse occurs when the upper inverter leg switch is the off state with a duration t_n^* calculated as follows:

$$t_n^* = \left(\frac{T_c}{2}\right)\left(1 - \frac{v^*}{\frac{V_{dc}}{2}}\right). \tag{21}$$

Substituting the modulation wave peak value of the modulator under investigation in the above formula and selecting the minimum pulse width equal to $2t_d$, the practical maximum linear modulation index $M_{i\max}^p$ can be found as follows:

$$M_{i\max}^p = \left(1 - k\frac{2t_d}{T_c}\right) * M_{i\max}^t. \tag{22}$$

In the above formula, $M_{i\max}^t$ is the theoretical linearity limit of the modulator. The k coefficient distinguishes the discontinuous PWM methods from the continuous-wave modulation methods. Its value is $k = 1$ for the DPWM methods and $k = 2$ for the modulators with continuous modulation wave. The small k coefficient of the DPWM methods indicates that DPWM methods have a wider voltage linearity range than SPWM, SVPWM, and other continuous-wave PWM methods. This result is a consequence of the different distribution of the inverter zero states in the two different modulation groups. The discontinuous PWM methods generate only one inverter zero state per carrier cycle (t_0: all the lower inverter switches are in the on state or t_7: all the upper switches are in the on-state), while the continuous PWM methods generate two zero states (for SVPWM $t_0 = t_7$). Since the total zero state time is not a function of the zero-sequence signal, but the line–line reference voltage, for the same line–line output voltage and carrier frequency value, the gate pulses of the DPWM methods are wider than the gate pulses of the modulators with continuous modulation waves. Therefore, the narrow pulse problem occurs at a higher modulation index with DPWM methods than continuous PWM methods.

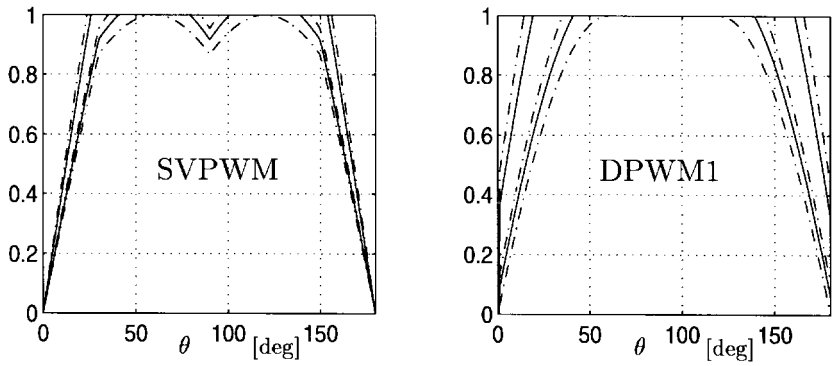

Fig. 11. Overmodulation region modulation wave profiles of SVPWM and DPWM1 for five different M_i^* values.

Notice that in both continuous and discontinuous PWM cases, the linearity boundaries depend on the ratio of the blanking time to the carrier cycle. Since the increasing carrier cycle practically implies increasing inverter power and increasing blanking time, the ratio is at least a few percent in most PWM-VSI drives. As a result, in most applications the linearity range of a modulator is reduced by a nonnegligible amount. In either modulation method, once beyond the boundary of linear modulation range, the output voltage is reduced by an amount which depends on the overlap time "×" shown in Fig. 12(c). As a result, the gain begins to decrease at a lower modulation index than the theoretical linearity limit and decreases more rapidly than the theoretical gain characteristic. Compared to the modulator theoretical gain reduction, the gain reduction of the DPWM methods due to the blanking time is fairly small and can be ignored for inverters with a few kilohertz switching frequency and blanking time less than a few microseconds [18]. In the gate-turn-off (GTO) switching-device-based PWM-VSI applications, the effect is more emphasized due to the long blanking time.

In certain applications, the narrow voltage pulses which occur at high-modulation levels may damage the drive or load. In such cases, the blanking time correction algorithm yields to a MPW control algorithm. For example, the switching device turn-on and/or turn-off speed capabilities of a GTO may not be sufficient to generate such narrow pulses. In order to avoid commutation failure of GTO-based drives, such narrow pulses are either eliminated or fixed at an acceptable level. Narrow voltage pulses can also cause overvoltage related motor insulation failure. State-of-the-art PWM-VSI drives utilize the modern third-generation IGBT devices with very small turn-on and turn-off times. Feeding motors with long cables from such PWM-VSI drives, significant overvoltages are generated across the motor terminals due to voltage reflection. As a result, the motor terminals experience excessive overvoltages contributing to insulation failure. When such PWM-VSI drives operate at high-modulation levels and narrow pulses are generated, the voltage-reflection problem is exacerbated: overvoltages in excess of twice the dc-bus value can appear across the terminals of a motor connected to a drive through as short a cable as 30 m [20]. Therefore, narrow voltage pulses are problematic in many PWM-VSI drives. These problems can be eliminated by either employing passive solutions such as inserting reactors between the drive and the motor, or active solutions such as MPW control which only requires modification to the PWM algorithm of a drive. The active solution is more economic, compact, and maintenance free.

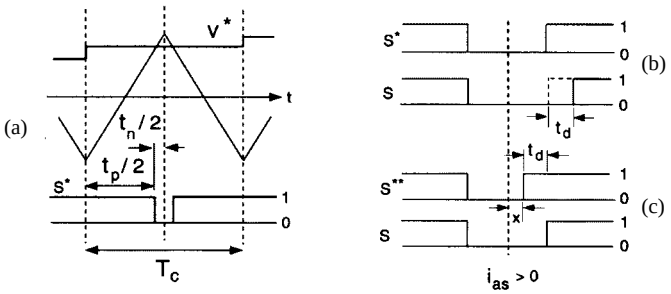

Fig. 12. Regular sampling PWM reference and gate signals. (a) The reference gate signal at high-modulation level. (b) No compensation results in asymmetric gate signal (for $i_{\rm as} > 0$). (c) Signal after exact compensation.

When employed, MPW control algorithms affect the modulator voltage gain and reduce the linear modulation range noticeably. The pulse elimination method (PEM) omits pulses narrower than a desirable limit and increases the modulator gain. The pulse limiting method (PLM) limits the width of the pulses to the minimum allowable pulse width limit and reduces the gain. However, as the modulation index increases, the modulator theoretical gain characteristics dominate, and in both cases the gain decreases rapidly, therefore, the gain curves follow the gain curves of Fig. 9 closely. In either method, the linearity limit of a modulator becomes smaller than the theoretical limits. In a proper design, the MPW pulses are wider than $2t_d$, therefore, the blanking time controller has no influence on the modulator linearity in this case. When MPW is applied, the practical voltage linearity limit of an inverter can be found from (22) by substituting the minimum pulse time $t_{\rm MPW}$ instead of $2t_d$. Since in this algorithm both sides of the triangle are affected while in the blanking time compensation case only one side of the triangle has incorrect gate signal, the effect of MPW control has more influence on the gain characteristic of a PWM-VSI. In particular, in GTO-based high-power PWM-VSI's which employ GTO's with large MPW values ($t_{\rm MPW} \approx 200\ \mu$s), MPW control starts at very low-modulation depths, and the nonlinear gain characteristics dominate the drive behavior at a low-modulation depth. Although less significant,

the effect cannot be underemphasized in the modern IGBT device-based PWM-VSI drives. In order to avoid the above-mentioned overvoltage problem, MPW times as large as 8–16 μs are required [20]. Since the carrier frequency is at least a few kilohertz, the influence of MPW control on the gain characteristics of such drives is significant.

The MPW-controlled modulator gain formulas can be closed-form calculated by modifying the theoretical modulator gain formulas [18]. For example, when employing PEM, the modulation index relations of the DPWM1 method become as follows [18]:

$$M_i' = M_i + 2(\cos\alpha_{m0} - \cos\alpha_{m1}) - M_i^* \frac{3}{\pi}(\alpha_{m1} - \alpha_{m0}) + M_i^* \frac{\sqrt{3}}{\pi}\left(\sin\left(2\alpha_{m1} + \frac{\pi}{6}\right) - \sin\left(2\alpha_{m0} + \frac{\pi}{6}\right)\right). \quad (23)$$

In the above equation, $M_i^{'}$ is the output-voltage modulation index and M_i is the theoretical modulation index value without MPW control which is given by (12). The intermediate variables α_{m0} and α_{m1} are calculated as follows:

$$\alpha_{m0} = -\frac{\pi}{6} + \arcsin\left(\frac{\pi}{2\sqrt{3}M_i^*}\left(1 - \frac{t_{\mathrm{MPW}}}{T_c}\right)\right) \quad (24)$$

$$\alpha_{m1} = -\frac{\pi}{6} + \arcsin\left(\frac{\pi}{2\sqrt{3}M_i^*}\right). \quad (25)$$

Fig. 13 shows the closed-form-calculated gain characteristics of PEM-controlled PWM-VSI for both SVPWM and DPWM1 [18]. Both modulators employ $f_c = 5$ kHz and $t_{\mathrm{MPW}} = 12$ μs. As the figure illustrates, the influence of the MPW algorithm has a nonnegligible effect on the voltage gain of SVPWM. The nonlinearity is noticeably smaller in the DPWM1 case. On the same figure, the blanking-time-dependent gain characteristic of DPWM1 is shown for $t_d = 4$ μs. Notice the blanking time has very little influence on the linearity compared to MPW. The gain curves of the PEM-controlled drive clearly indicate the linearity range of DPWM methods is significantly wider than SVPWM, and in the overmodulation region, DPWM1 is the only modulator that maintains a high gain. Therefore, DPWM1 can be most beneficial to high-power PWM-VSI drives and all the PWM-VSI drives with large $\frac{t_{\mathrm{MPW}}}{T_c}$ ratio while operating in the high-modulation range.

VI. Voltage-Gain Linearization

As illustrated in Fig. 14(a) in block diagram form, in the overmodulation region the VSI output voltage is different from the reference voltage due to gain nonlinearity. PWM-VSI drives which employ PLM and drives which do not employ any MPW control algorithm always experience gain reduction, while those employing PEM experience gain increase in the entrance of the overmodulation region and gain reduction as the overmodulation region is further penetrated. On the other hand, it is important to program the reference fundamental component voltage value correctly so that the drive performance does not degrade. For example, in ac motor drive applications the stator flux value (or equivalently the $\frac{V}{f}$ value) must be maintained at a proper level to obtain high efficiency.

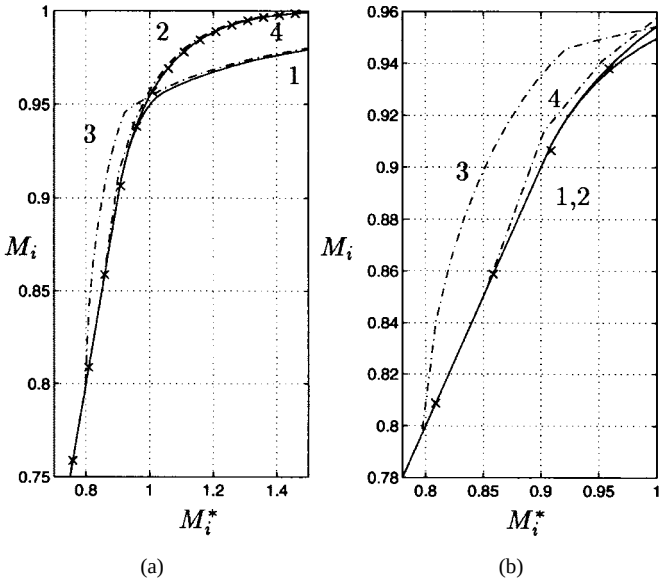

Fig. 13. (a) SVPWM and DPWM1 theoretical $M_i = f(M_i^*)$ characteristics and (b) the magnified view in the low end of the overmodulation region. 1: SVPWM, 2: DPWM1, 3: SVPWM with MPW, and 4: DPWM1 with MPW. The blanking-time-dependent nonlinearity of DPWM1 is shown with the "×" symbol.

Therefore, fundamental component voltage linearity must be retained in the overmodulation range also. Since the discussed modulation methods have nonlinear gain characteristics, to retain voltage linearity, a gain compensation technique must be employed. Gain compensation techniques are based on either adding extra signals such as square waves to the reference modulation waves or by increasing or decreasing the fundamental component magnitude of the reference modulation waves [3]. As shown in Fig. 14(b), in the latter approach the reference modulation wave fundamental component signal is premultiplied with the inverse gain function such that the nonlinearity is canceled. The former approach may alter the modulator harmonic characteristics while the latter does not. In this work, the inverse gain method will be investigated.

In both gain linearization methods, calculating the gain compensation function is very difficult. The difficulty of describing the gain functions in closed-form equations has been overcome in the early stages of this paper. However, closed-form calculation of the inverse gain function is very difficult. Furthermore, on-line computation of such complex gain compensation signals with the state-of-the-art DSP or μP devices is prohibitive. Instead, the gain function and its inverse can be numerically computed off line, and the data can be utilized to approximate the gain compensation function by a lookup table and/or a simple curve-fitting method.

Inverse gain compensation-based gain linearization of the SPWM method which employs a table lookup approach was previously reported, and the requirement for a large table size and an efficient table search algorithm was indicated [3]. The zero-sequence injection PWM methods which are discussed in this paper have a smaller gain range than SPWM, therefore, the memory requirements are less demanding. However, of all the discussed methods, DPWM1 provides an exceptional implementation advantage due to its significantly small gain

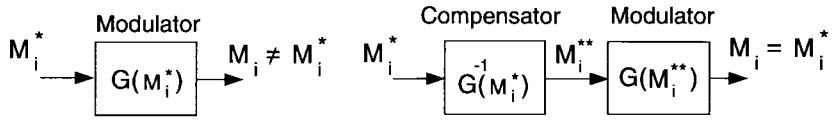

(a) (b)

Fig. 14. Overmodulation range voltage-gain block diagrams. (a) Modulator nonlinear gain characteristic. (b) The compensator cancels the nonlinearity by inverse gain multiplication.

reduction. The gain compensation signal (inverse gain function magnitude) of DPWM1 is less than two units while the other modulators require large signals ranging from 5 to 20 units. Therefore, when employing DPWM1 in a fixed-point digital platform, the word length of the μP or DSP can be more efficiently utilized. The other methods require a significant amount of data shifting to process the large inverse gain values such that overflow does not occur, and this results in poor modulation signal resolution and increased computation time. The inverse gain function data of DPWM1 can be easily fit into several first-order polynomials leading to a smaller memory size requirement and improved accuracy. Near the six-step operating point ($M_i \geq 0.99$), the gain inverse coefficients increase due to the rapid gain reduction and the inverse gain function can be better modeled by several data entries.

Employing the analytical gain function of DPWM1 and accounting for PEM-based nonlinearity [18], the inverse gain function data can be accurately and easily computed from (23). Utilizing this data to obtain a simple hybrid model consisting of several piecewise first-order polynomial functions and several data entries is a straightforward task.

Compared to the direct digital PWM implementation, the triangle-intersection technique requires simpler overmodulation algorithms. In the direct digital method, the overmodulation condition is detected only after computing a zero-state time length with negative sign. Therefore, a back step for correcting the sign is inevitable, and additional algorithms (often complex) must be employed to compensate for the gain loss [6]. Therefore, the DPWM1 triangle-intersection method requires the simplest overmodulation algorithm and has superior performance when compared to all the other PWM methods reported.

VII. Waveform Quality and Switching Losses

The linear modulation range harmonics of carrier-based PWM methods (characteristic harmonics) are concentrated at the carrier frequency and its sidebands. In the overmodulation region, as the unmodulated portions of the modulation waves increase, the characteristic harmonics decrease. However, large amounts of subcarrier frequency harmonics (5th, 7th, etc.) are generated, and as the six-step mode is approached, these harmonics become increasingly dominant in determining the waveform quality. In this section, the linear modulation and overmodulation region waveform quality factor of the discussed modulators is investigated.

In the high end of the linear modulation range, the waveform quality of DPWM methods is superior to SVPWM and other PWM methods with continuous modulation wave, and the opposite is true in the low-modulation range [8]. Therefore, a high-performance drive must select SVPWM in the low-modulation region and make a transition to DPWM methods beyond a certain modulation level. The proper transition modulation index value can be found from the intersection point of the modulation index versus waveform quality factor curves of the selected methods. Defined in the following, the inverter output line–line voltage weighted total harmonic distortion (WTHD) factor is an appropriate measure in determining the modulator waveform quality both in the linear and overmodulation range [18]

$$\text{WTHD} = 100 \times \frac{\sqrt{\sum_{i=2}^{n} \left(\frac{V_{\text{LL}i}}{i}\right)^2}}{V_{\text{LL1}}}. \tag{26}$$

In most ac motor drive and utility interface applications, the WTHD function is more meaningful than the conventional voltage THD definition in which the $\frac{1}{i}$ weight factor is absent in the formula because the WTHD function accounts for the low-pass filter characteristic of the load inductance automatically. Hence, a better measure for the current harmonic distortion. The WTHD function is carrier frequency dependent, and the V_{LLi} terms are typically calculated by evaluating the PWM-VSI line–line output-voltage data for one fundamental cycle (obtained by simulation) through fast Fourier transformation (FFT) analysis.

In this study, line–line voltage WTHD curves for SVPWM and DPWM1 are calculated and compared. The inverter line–line voltage data of a PWM-VSI drive which employs the once per carrier regular sampling technique is generated by means of computer simulations. The simulation assumes a fundamental frequency of $f_e = 60$ Hz. The carrier frequency f_c is 5 kHz in the DPWM1 case and 3.33 kHz in the SVPWM case. This implies equal inverter average switching frequency in both methods. In order to illustrate the carrier frequency dependency of the WTHD function, the SVPWM case is evaluated for 5 kHz also. The harmonic voltages, accounting for all the dominant harmonics (up to $3f_c$), were calculated by evaluating the 8192 data points by means of an FFT algorithm of the MATLAB numerical software package.

The WTHD curves in Fig. 15(a) illustrate the advantageous waveform characteristics of the DPWM1 method at high modulation including the overmodulation range. Under the equal inverter average switching frequency criteria, the harmonic distortion of DPWM1 is less than the SVPWM methods from $M_i \approx 0.6$ to $M_i \approx 0.95$, where both curves merge. Under an equal carrier frequency criteria, which implies a 50% increase in the average switching frequency in the SVPWM case, the waveform quality advantage of SVPWM over DPWM1 is lost near $M_i \approx 0.90$.

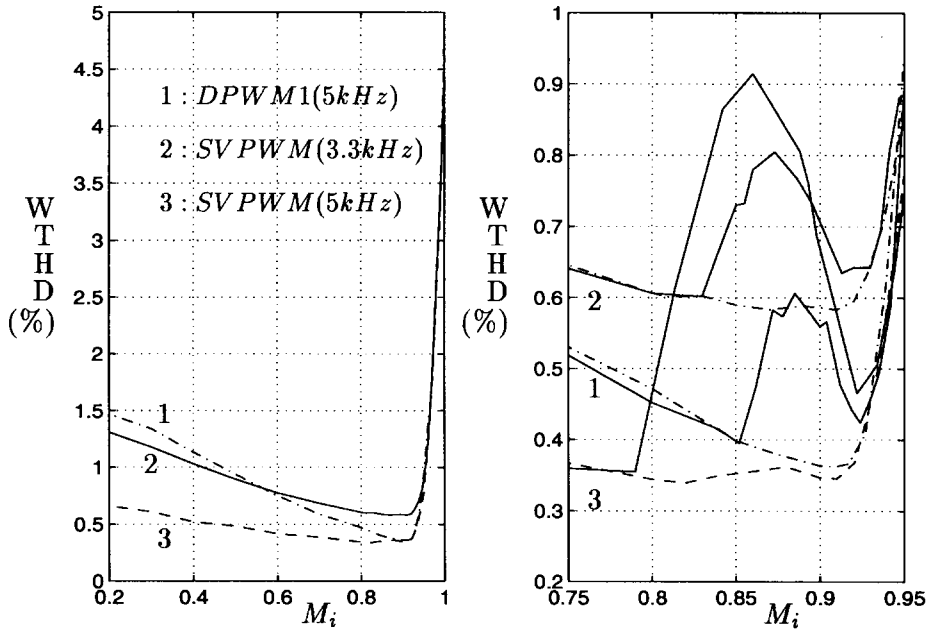

Fig. 15. WTHD characteristics of SVPWM and DPWM1. (a) Ideal inverter model case. (b) Magnified view with MPW (—) and without MPW (- - -) control algorithm.

The blanking time and MPW control-algorithm-dependent inverter nonlinearities can cause significant harmonic distortion increase which is modulator dependent. Fig. 15(b) illustrates the increase in the harmonic distortion when a 12-μs MPW control algorithm is employed in the above system. Although the harmonic distortion increases in all the cases, the relative increase in the DPWM1 case is significantly smaller than the SVPWM's. The data clearly indicates that the harmonic distortion of the SVPWM method significantly increases and the increase in the switching frequency worsens the harmonic distortion. Therefore, accounting for the MPW nonlinearity, the superiority of DPWM1 over SVPWM begins at a significantly smaller modulation index value than the ideal case. Fig. 15(b) clearly indicates that if the carrier frequency is kept constant and the modulation method is switched from SVPWM to DPWM1 beyond $M_i \approx 0.8$, no degradation of waveform quality will be obtained relative to the SVPWM case. Furthermore, the switching losses are greatly reduced.

Fig. 15 also indicates the overmodulation region waveform characteristics of DPWM1 are superior to SVPWM until the point where the 5th, 7th, etc., subcarrier frequency harmonics totally dominate and both WTHD curves merge $(M_i \approx 0.95)$. Although in the low end of the overmodulation range the WTHD factor is strongly dependent on the carrier frequency, inverter nonlinearities, and the modulation method, in the high end it is dominated by the subcarrier frequency harmonics, and it is weakly dependent on the carrier frequency and the modulation method [18]. Since the subcarrier frequency harmonics do not play an important role in determining the modulator waveform quality, the performance evaluation should mainly be based on the low-end overmodulation range waveform quality, and clearly this argument favors DPWM1 due to its superior voltage-gain characteristics.

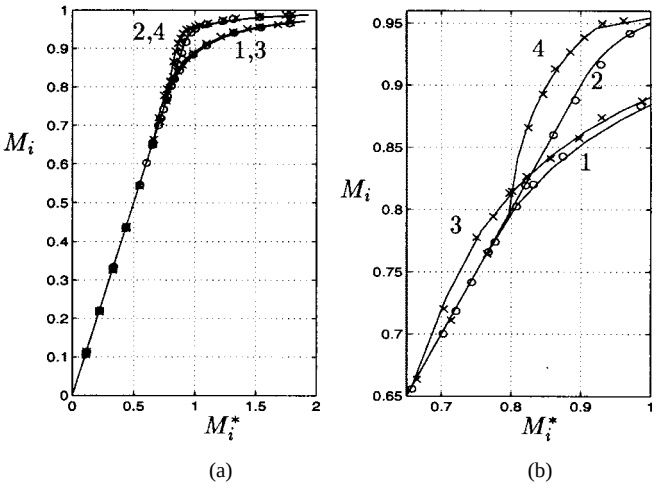

Fig. 16. Experimental and theoretical $M_i = f(M_i^*)$ characteristics of SPWM and SVPWM. (a) Full modulation range. (b) Magnified view of the nonlinear modulation region. 1: SPWM, 2: SVPWM, 3: SPWM with MPW, and 4: SVPWM with MPW. The experimental data is shown with "o" and "×" symbols, while the continuous curves correspond to the theoretical formulas.

In the high end of the linear modulation region, the waveform quality of DPWM2 is only slightly better than DPWM1, therefore, the choice between the two modulators can be based on the switching loss minimization criteria [8]. The switching losses of the drive can be reduced by selecting DPWM1 for near unity-power-factor loads and DPWM2 for near 30° lagging loads because with this modulator choice the unmodulated portions of each modulation wave coincide with the largest current conducting intervals of the corresponding drive phase. At the DPWM linear modulation limit, regardless the load value, DPWM1 should be selected in order to obtain high-voltage gain in the overmodulation region. Since the

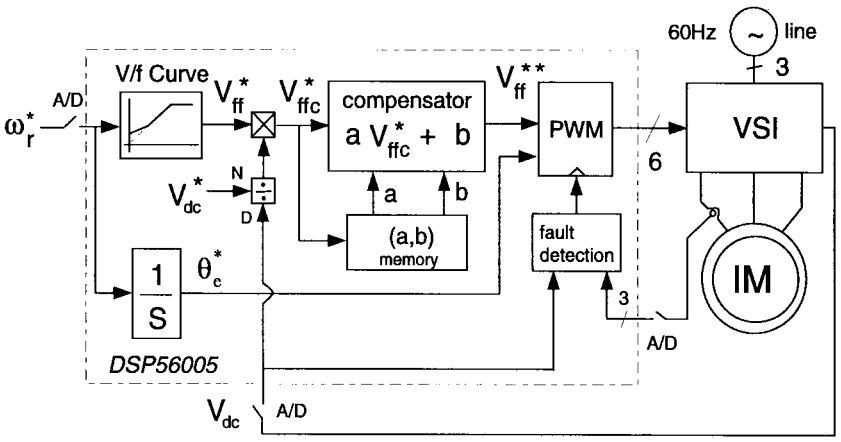

Fig. 17. The experimental setup and the gain linearized DPWM1-based $\frac{V}{f}$-controlled motor drive block diagram.

overmodulation range waveform quality of all the DPWM methods is practically the same, DPWM1 is invariably the optimal overmodulation modulator [18]. Generating all the discussed modulation waves in fully digital triangle-intersection implementation-based digital platforms is an easy task. Programming several modulators by employing the low-cost high-performance state-of-the-art DSP's or μP's and on-line selecting a modulation method depending on the modulation index is a feasible approach.

VIII. Experimental Results

In this section, the experimental voltage-gain characteristics of SPWM, SVPWM, and DPWM1 are extracted, and their waveform characteristics are illustrated. For this purpose, an experimental system which consists of a PWM-VSI drive and a 10-HP induction machine has been utilized. The inverter drive employs triangle-intersection technique-based PWM, and the carrier frequency is 5 kHz. The blanking time of the inverter is 4 μs. The controller is fully digital, and it employs a 24-b fixed-point DSP (Motorola 56 005) with 40-MHz clock frequency.

For the purpose of voltage-gain measurement, operating the drive in the constant V/f mode is adequate, and the motor can be operated at no load. The V/f algorithm and the modulation waves are generated by the DSP. In particular, generation of all the discussed modulation waves, exact blanking time compensation, and required MPW control are all simple tasks requiring only a few lines of software code when employing a DSP. The digitally implemented triangular comparison hardware (PWM block) is also inside the DSP chip providing a compact integrated solution.

First, the SPWM and SVPWM method voltage-gain characteristics were extracted by measuring the reference and output line–line voltages from zero voltage until the six-step mode is reached. The inverter output-voltage fundamental component value was measured by a dynamic signal analyzer (HP35670A). The inverter dc-bus voltage was also measured in order to account for the utility line and load-dependent dc-bus voltage variations. The test was conducted with and without PEM-based MPW control algorithm. When employed, PEM eliminates (drops) the pulses which are narrower than 12 μs. Experimental results are shown in Fig. 16 along with the analytical results. As the figure clearly indicates, the theoretical and experimental results match with good accuracy. The SVPWM method has wider linearity range than the SPWM method, and both methods require very large reference signals in order to reach the six-step mode. As the experimental data indicates, PEM narrows the linearity range of both modulators quite significantly.

In the second stage, the gain characteristics of DPWM1 were measured—first without PEM control and second with 12-μs PEM control. In the following, an inverse gain algorithm was implemented for the PEM-controlled case and gain data extracted. Selecting the MPW length as 12 μs, the inverse gain function data was computed from (23), and this data was utilized to extract the following numerical approximation for the inverse gain compensated modulation index function:

$$M_i^{**}(M_i^*) = \begin{cases} M_i^* & 0 < M_i^* < 0.852 \\ 0.5252M_i^* + 0.4026 & 0.852 < M_i^* < 0.88 \\ 1.0823M_i^* - 0.0887 & 0.88 < M_i^* < 0.91 \\ 1.6659M_i^* - 0.6191 & 0.91 < M_i^* < 0.94 \\ 3.4396M_i^* - 2.2903 & 0.94 < M_i^* < 0.97 \\ 7.9754M_i^* - 6.6882 & 0.97 < M_i^* < 0.99 \\ 1.247 & 0.99 < M_i^* < 0.992 \\ 1.285 & 0.992 < M_i^* < 0.994 \\ 1.335 & 0.994 < M_i^* < 0.996 \\ 1.422 & 0.996 < M_i^* < 0.998 \\ 1.49 & 0.998 < M_i^* < 0.999 \\ 1.547 & 0.999 < M_i^* < 0.9993 \\ 1.65 & 0.999 < M_i^* < 0.9995 \\ 1.81 & 0.9995 < M_i^* < 1.0. \end{cases} \tag{27}$$

The above numerical representation provides a straightforward and highly accurate approximation with little computation and memory requirements, suitable for the μP or DSP implementations. In the gain-linearized case, a dc-bus voltage-disturbance decoupling algorithm which scales the reference modulation index by $\frac{V_{\rm dc}^*}{V_{\rm dc}}$ was also implemented in order to account for the dc-bus voltage variations. The $\frac{V_{\rm dc}^*}{V_{\rm dc}}$

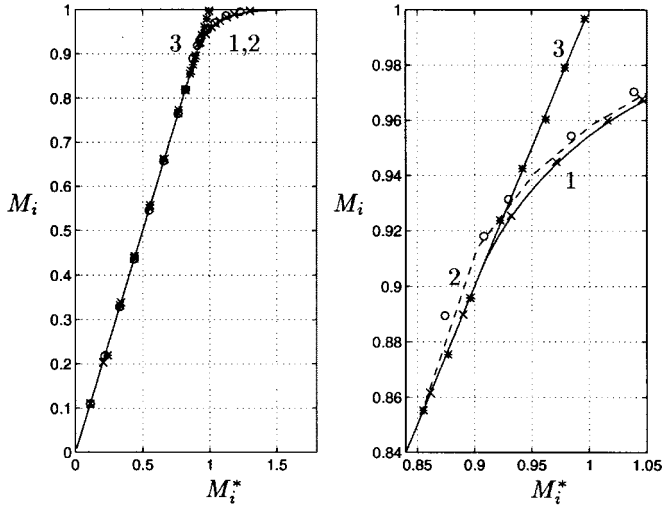

(a) (b)

Fig. 18. (a) Experimental and theoretical $M_i = f(M_i^*)$ characteristics of DPWM1 with and without linearization and (b) the magnified view of the overmodulation region. 1: The theoretical $M_i = f(M_i^*)$ curve. 2: The theoretical $M_i = f(M_i^*)$ curve with MPW. 3: Ideal linear modulator line. The experimental results are shown with "o," "×," and "∗" symbols.

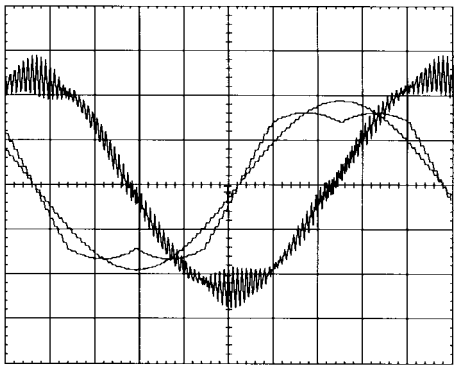

Fig. 19. Experimental SVPWM modulation wave, its fundamental component, and the motor current waveforms for $M_i^* = 0.75$. Scales: 2 ms/div, 2 A/div, and 5 V/div.

value was computed by a simple Taylor series approximation ($\frac{1}{1+x} \approx 1 - x + x^2$) instead of straightforward division which consumes a significant amount of computations. The complete block diagram of the system for this case is shown in Fig. 17.

Fig. 18 shows the theoretical and experimental gain characteristics of the DPWM1 method. The linearity range of the DPWM1 method as the data indicates is wider than the SVPWM case, and the influence of the MPW algorithm is significantly smaller. The gain compensator, as shown in the figure extends the modulator linearity until near the six-step operating mode with high accuracy.

For the purpose of comparing the waveform quality of DPWM1 and SVPWM, the motor currents for several modulation index values are demonstrated along with the modulation waveforms. The modulation signals were output from the DSP through a digital-to-analog (D/A) converter and the triangular wave gain is $\frac{20\ \mathrm{V}}{V_{\mathrm{dc}}^*}$ (± 10 V represent the positive/negative dc rail clamp conditions). Figs. 19 and 20 illustrate the motor

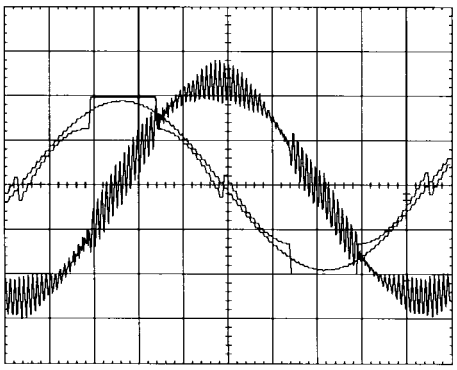

Fig. 20. Experimental DPWM1 modulation wave, its fundamental component, and the motor current waveforms for $M_i^* = 0.75$ value. Scales: 2 ms/div, 2 A/div, and 5 V/div.

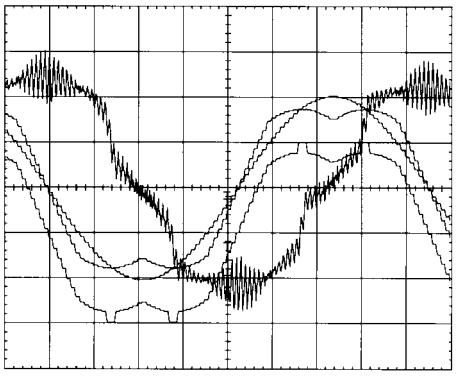

Fig. 21. Experimental SVPWM modulation wave, modulation signal previous to MPW block, its fundamental component, and the motor current waveforms for $M_i^* = 0.82$. Note the low-frequency current harmonic distortion. Scales: 2 ms/div, 2 A/div, and 5 V/div.

current and modulation waveforms of SVPWM and DPWM1 for $M_i^* \approx 0.75$. As the figures indicate, both modulators have good waveform quality within the linear modulation range, and the ripple of SVPWM is slightly less. However, as the modulation index is increased and MPW control is applied, the SVPWM performance degrades significantly. Fig. 21 shows when a 12-μs PEM is employed, the SVPWM method performance degrades at $M_i^* \approx 0.82$, a value significantly smaller than the theoretical linearity limit (0.907). The modulator linearity is lost at $M_i^* \approx 0.82$, and the current waveform contains significant low-frequency harmonic distortion leading to poor motor performance. As illustrated by the $M_i^* \approx 0.855$ operating point in Fig. 22, DPWM1 maintains linearity and low harmonic distortion in a significantly wider modulation range. As illustrated in Fig. 23 by the $M_i^* \approx 0.876$ operating point, beyond $M_i^* \approx 0.855$, modulator linearity is lost and the waveform quality significantly degrades. A further increase in the modulation index results in significant increase of the low-frequency subcarrier harmonic content. Fig. 24 illustrates the near six-step mode behavior of the inverter.

Notice in all the figures which belong to the high-modulation region that the PWM ripple current magnitude appears to be practically the same. Since the carrier frequency is fixed at 5 kHz for both SVPWM and DPWM1, the average switching frequency of DPWM1 is 33% less than SVPWM.

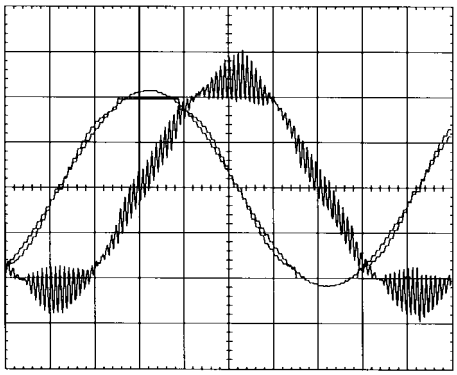

Fig. 22. Experimental DPWM1 modulation wave, its fundamental component, and the motor current waveforms for $M_i^* = 0.855$ value. Scales: 2 ms/div, 2 A/div, and 5 V/div.

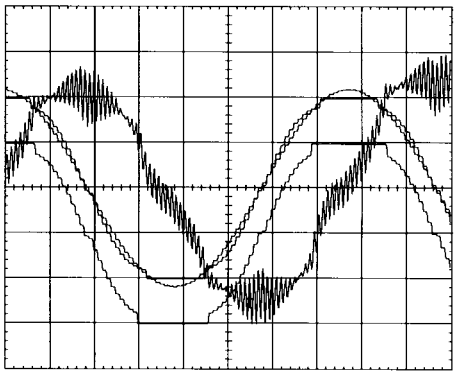

Fig. 23. Experimental DPWM1 modulation wave, modulation signal previous to MPW block, its fundamental component, and the motor current waveforms for $M_i^* = 0.876$. Scales: 2 ms/div, 2 A/div, and 5 V/div.

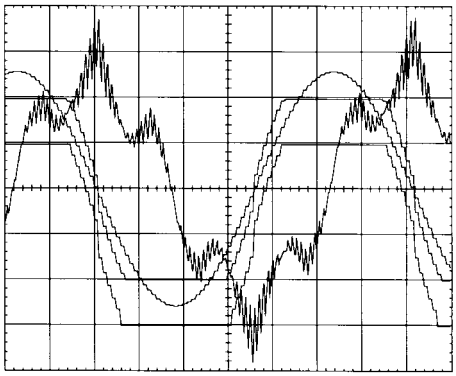

Fig. 24. Experimental DPWM1 modulation wave, modulation signal previous to MPW block, and the motor current waveforms for $M_i^* = 0.964$. Note near the six-step mode the low-frequency subcarrier harmonics are dominant. Scales: 2 ms/div, 2 A/div, and 5 V/div.

Therefore, DPWM1 has significantly reduced switching losses compared to SVPWM. Considering the reduction in the switching losses and increase in the linear modulation range, the DPWM1 method clearly becomes the choice for operating in the high-modulation range.

Finally, the sensitivity of the V/f-controlled drive to dc-bus voltage variations is illustrated with and without the inverse gain compensation and dc-bus disturbance decoupling algorithms. The V/f-controlled induction machine was operated at constant inverter output-voltage reference value $V_{1m}^* = 337$ V ($M_i^* = 0.855$ at $V_{\rm dc}^* = 620$ V). Obtained from a diode rectifier, the dc-bus voltage of the drive was slowly varied by adjusting the ac-input voltage via an autotransformer, and the motor terminal voltage was measured. Fig. 25 illustrates the experimental inverter output-voltage dc-bus voltage characteristics with and without inverse gain compensation and dc-bus voltage-disturbance decoupling. As the figure indicates, the compensated case output voltage is maintained at the commanded value until the dc-bus voltage is significantly reduced, and the inverter operates in the six-step mode. The uncompensated case output voltage significantly changes with the dc-bus voltage variation. The motor speed and torque deviate from the normal operating points, and poor drive performance results. Therefore, the compensated drive performance is insensitive to the dc-bus voltage variations for a wide range of dc-bus voltage variations (utility-line voltage sag or surge conditions), while the uncompensated drive experiences disturbances.

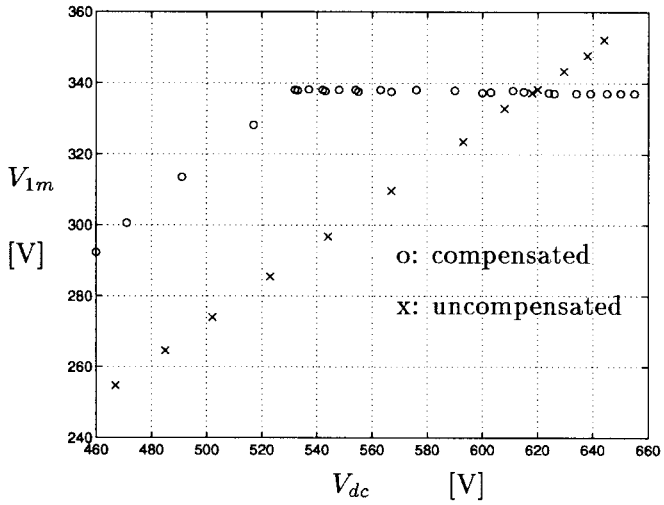

Fig. 25. Terminal-voltage dc-bus voltage characteristics for $V_{1m}^* = 337$ V.

IX. Current-Controlled Drives

High-performance field-orientation-controlled (FOC) drives and voltage-source converter (VSC) utility interface applications generally employ high-bandwidth current-control algorithms and in such applications dynamic performance requirements are demanding. Although the conventional high-performance current controllers and the PWM methods have satisfactory linear modulation range performance, the overmodulation range performance is poor. Since in the overmodulation range the feedback currents contain considerable amount of subcarrier frequency harmonics, in addition to the inherent modulator/inverter subcarrier frequency harmonics, feedback harmonic current-dependent harmonics are generated. Performance degradation is generally significant, and the overmodulation operating region is often prohibited except for dynamic conditions.

Since the gain compensation technique provides "per fundamental cycle volt-second balance," in this technique intentional reference output-voltage errors are generated within well-defined intervals of the fundamental cycle. On the other hand, to obtain high dynamic performance (to manipulate the dynamic condition rapidly), the voltage error must be minimized in every carrier cycle [21]. Therefore, the inverse gain compensation technique does not guarantee high dynamic performance, and high modulator gain does not guarantee superior dynamic overmodulation performance. However, by employing DPWM methods in the higher end of the linear modulation region, the carrier-based current-controlled PWM-VSI drives can benefit from the high-performance characteristics of DPWM methods, and the influence blanking time and MPW control algorithm on voltage linearity range can be significantly reduced. The dynamic overmodulation issues of high-performance current controllers and PWM algorithms are beyond the scope of this paper, and they are reported in [18].

X. Conclusion

Closed-form voltage-gain formulas of the conventional carrier-based PWM methods, which are very useful tools in the analysis and design of PWM-VSI drives have been derived. High-modulation index operating range voltage-gain characteristics of various conventional carrier-based PWM methods have been analyzed and comparative results provided. The study indicates the DPWM methods have wider linearity range than the continuous PWM methods. The overmodulation range performance characteristics of DPWM1 are shown to be superior to the remainder of the known modulators. The voltage gain of DPWM1 is exceptionally high, and the harmonic distortion is low.

It is shown that the inverter blanking time and MPW control-based nonlinearities can significantly influence voltage gain and harmonic distortion characteristics of a modulator. MPW control significantly reduces the linearity range and increases the harmonic distortion. The effect is less significant in the discontinuous PWM methods compared to the conventional SPWM and SVPWM methods.

The study indicates that for best overall performance, a combination of two different modulators must be employed: in the low-modulation index range SVPWM has lower harmonic distortion. In the high-modulation index range, DPWM methods have wider linearity and less harmonic distortion. In the overmodulation region, DPWM1 is the best solution.

Voltage-gain linearization is a simple task with DPWM1, and a polynomial curve-fit-based inverse gain function in most of the region and a small table entry near six step were found to be adequate to provide good linearity in the overmodulation range.

Experimental gain characteristics are in good agreement with the theoretical predictions and illustrate the performance superiority of DPWM1 over SVPWM in the high-modulation and overmodulation ranges. The inverse gain compensation and dc-bus disturbance decoupling algorithms linearize the modulator with high accuracy and result in high-drive performance.

References

[1] A. Schönung and H. Stemmler, "Static frequency changers with subharmonic control in conjunction with reversable variable speed ac drives," in *Brown Boveri Rev.*, vol. 51, nos. 8/9, pp. 555–577, Sept. 1964.

[2] H. Van Der Broeck, H. Skudelny, and G. Stanke, "Analysis and realization of a pulse width modulator based on voltage space vectors," in *IEEE-IAS Conf. Rec.*, 1986, pp. 244–251.

[3] R. J. Kerkman, T. M. Rowan, D. Leggate, and B. J. Seibel, "Control of PWM voltage inverters in the pulse dropping region," in *IEEE-APEC Conf. Rec.*, 1994, pp. 521–528.

[4] T. M. Rowan, R. J. Kerkman, and T. A. Lipo, "Operation of naturally sampled current regulators in the transition mode," *IEEE Trans. Ind. Applicat.*, vol. IA-23, pp. 586–596, July/Aug. 1987.

[5] S. Bolognani and M. Zigliotti, "Novel digital continuous control of SVM inverters in the overmodulation range," in *IEEE-APEC Conf. Rec.*, 1996, pp. 219–223.

[6] J. Holtz, W. Lotzkat, and A. Khambadkone, "On continuous control of PWM inverters in the overmodulation range including the six-step mode," in *IEEE-IECON Conf. Rec.*, 1992, pp. 307–322.

[7] S. Ogasawara, H. Akagi, and A. Nabae, "A novel PWM scheme of voltage source inverter based on space vector theory," in *European Power Electronics Conf. Rec.*, 1989, pp. 1197–1202.

[8] H. W. Van Der Broeck, "Analysis of the harmonics in voltage fed inverter drives caused by PWM schemes with discontinuous switching operation," in *European Power Electronics Conf. Rec.*, 1991, pp. 261–266.

[9] J. Holtz, "Pulsewidth modulation for electronic power conversion," *Proc. IEEE*, pp. 1194–1214, Aug. 1994.

[10] G. Buja and G. Indri, "Improvement of pulse width modulation techniques," *Archiv für Elektrotechnik, 57*, pp. 281–289, 1975.

[11] M. Depenbrock, "Pulse width control of a 3-phase inverter with nonsinusoidal phase voltages," in *IEEE-ISPC Conf. Rec.*, 1977, pp. 399–403.

[12] J. Schörner, "Bezugsspannung zur umrichtersteuerung," in *ETZ-b, Bd. 27*, 1975, pp. 151–152.

[13] K. G. King, "A three phase transistor class-b inverter with sinewave output and high efficiency," in *Inst. Elec. Eng. Conf. Publ. 123*, 1974, pp. 204–209.

[14] L. J. Garces, "Current control of field oriented ac induction motor drives," in *IEEE Tutorial: Mircoprocessor Control of Motor Drives and Power Converters*, 1993, pp. 5-1–5-46.

[15] J. W. Kolar, H. Ertl, and F. C. Zach, "Influence of the modulation method on the conduction and switching losses of a PWM converter system," *IEEE Trans. Ind. Applicat.*, vol. IA-27, pp. 1063–1075, Nov./Dec. 1991.

[16] K. Ogata, *Modern Control Engineering*. Englewood Cliffs, NJ: Prentice-Hall, 1970.

[17] S. R. Bowes and A. Midoun, "Suboptimal switching strategies for microprocessor controlled PWM inverter drives," *Proc. Inst. Elect. Eng.*, vol. 132, pt. B, no. 3, pp. 133–148, 1985.

[18] A. M. Hava, "Carrier based PWM-VSI overmodulation strategies," Ph.D. dissertation, Univ. Wisconsin, Madison, 1997.

[19] D. Leggate and R. J. Kerkman, "Pulse based dead-time compensator for PWM voltage inverters," in *IEEE-IECON Conf. Rec.*, 1995, pp. 474–481.

[20] R. J. Kerkman, D. Leggate, and G. Skibinski, "Interaction of drive modulation and cable parameters on ac motor transients," in *IEEE-IAS Conf. Rec.*, San Diego, CA, 1996, pp. 143–152.

[21] S. Jul-Ki and S. Sul, "A new overmodulation strategy for induction motor drive using space vector PWM," in *Applied Power Elect. Conf.*, Dallas, TX, Mar. 1995, pp. 211–216.

Ahmet M. Hava (S'91) was born in Mardin, Turkey, in 1965. He received the B.S. degree from Istanbul Technical University, Istanbul, Turkey, in 1987 and the M.S. degree from the University of Wisconsin, Madison, in 1990, both in electrical engineering. He is currently working toward the Ph.D. degree at the University of Wisconsin.

In 1995, he was with Rockwell Automation-Allen Bradley Company, Mequon, WI. He is currently with Yaskawa Electric America, Inc., Northbrook, IL. His research interests include power electronics, electric machines, and control.

Russel J. Kerkman (S'67–M'76–SM'88–F'98) received the B.S.E.E., M.S.E.E., and Ph.D. degrees in electrical engineering from Purdue University, West Lafayette, IN, in 1971, 1973, and 1976, respectively.

From 1976 to 1980, he was an Electrical Engineer at the Power Electronics Laboratory of Corporate Research and Development of the General Electric Company, Schenectady, NY. He is currently an Engineering Consultant at Rockwell Automation/Allen Bradley Company, Mequon, WI. His career includes 20 years of industrial experience in power electronics. His current interests include: modeling and control of general-purpose industrial drives, adaptive control applied to field-oriented induction machines, application of observers to ac machines, design of ac motors for adjustable-speed applications, and EMI from PWM inverters. He is a coholder of 15 patents, all in adjustable-speed drives.

Dr. Kerkman is the recipient of seven IEEE Prize Paper Awards. He is a Member of the Industry Applications Society, Industrial Electronics Society and Power Electronics Society.

Thomas A. Lipo (M'64–SM'71–F'87) received the B.E.E. and M.S.E.E. degrees from Marquette University, Milwaukee, WI, in 1962 and 1964 and the Ph.D. degree in electrical engineering from the University of Wisconsin, Madison, in 1968.

From 1969 to 1979, he was an Electrical Engineer at the Power Electronics Laboratory of Corporate Research and Development of the General Electric Company, Schenectady NY. He became a Professor of Electrical Engineering at Purdue University, West Lafayette, IN, in 1979. In 1981, he joined the University of Wisconsin in the same capacity, where he is presently the W.W. Grainger Professor for Power Electronics and Electrical Machines.

Dr. Lipo received the Outstanding Achievement Award in 1986 from the IEEE Industry Applications Society for his contributions to the field of ac drives. In 1990, he received the William E. Newell Award of the IEEE Power Electronics Society for contributions to the field of power electronics. He recently received the 1995 Nicola Tesla IEEE Field Award "for pioneering contributions to simulation of and application to electric machinery in solid-state ac motor drives." He served in various capacities for three IEEE Societies, including President of IAS in 1994.